Journal of
Applied
Crystallography
ISSN 0021-8898

Received 18 January 2005
Accepted 3 May 2005

The incompressibility and thermal expansivity of D_2O ice II determined by powder neutron diffraction

A. D. Fortes,[a]* I. G. Wood,[a] M. Alfredsson,[a] L. Vočadlo[a] and K. S. Knight[b,c]

[a]Research School of Geological and Geophysical Sciences, University College London, Gower Street, London WC1E 6BT, UK, [b]ISIS Facility, Rutherford Appleton Laboratory, Chilton, Didcot, Oxfordshire OX11 0QX, UK, and [c]Natural History Museum, Cromwell Road, London SW7 5BD, UK. Correspondence e-mail: andrew.fortes@ucl.ac.uk

Using high-resolution neutron powder diffraction, the molar volume of a pure sample of D_2O ice II has been measured, within its stability field, at 225 K, over the pressure range $0.25 < P < 0.45$ GPa. Ar gas was used as the pressure medium, to avoid the formation of 'stuffed ice' gas hydrates encountered when using He. The third-order Birch–Murnaghan equation of state parameters of helium-free D_2O ice II, referenced to 225 K, are: $V_{0,225} = 306.95 \pm 0.04$ Å^3 (1299.7 ± 0.2 kg m^{-3}), $K_{0,225} = 12.13 \pm 0.07$ GPa, with $K'_{0,225}$ fixed at 6.0. The thermal expansivity of metastable D_2O ice II samples recovered to ambient pressure has also been measured, over the range $4.2 < T < 160$ K; above 160 K an irreversible transition to ice I*c* was observed. The volumetric expansion coefficient, α_V, at $P = 0$ and $T = 225$ K, is predicted to be 2.48×10^{-4} K^{-1}.

1. Introduction

The crystalline polymorph of solid water called ice II is the stable phase at pressures of ∼0.2 GPa to ∼0.5 GPa and temperatures below ∼250 K (Fig. 1). Ice II was discovered and named by Tammann (1900) and studied further by Bridgman (1912, 1935, 1937), who established its equilibrium phase boundaries, specific volume differences, and entropy differences, with respect to ices I*h*, III and V. In common with many of the other known high-pressure phases, ice II is readily recoverable to atmospheric pressure after cooling to below ∼120 K. Hence, the first structural investigations were carried out upon decompressed samples: McFarlan (1936*a*,*b*) reported what he supposed to be the structure of ice II at 118 K and ambient pressure, using powder X-ray diffraction; however, his diffraction pattern appears to be that of ice IX. X-rays were subsequently applied to the analysis of the ice II structure by Kamb & Datta (1960), who published an incorrect indexing of their powder pattern in a cubic setting, and by Bertie *et al.* (1963), who presented the correct (triply primitive) hexagonal cell. The structure was solved, in space group $R\bar{3}$ ($Z = 12$), with $a = 7.78$ Å and $\alpha = 113.1°$ at 123 K, by Kamb (1964) using single-crystal X-ray diffraction, and inferred to be fully proton ordered. This interpretation was supported by features in the infrared spectrum (Bertie & Whalley, 1964), the lack of dielectric dispersion seen in the disordered phases (Wilson *et al.*, 1965), and the entropy difference between ice I*h* and ice II (Whalley & Davidson, 1965). The existence of complete orientational order was finally confirmed by powder neutron diffraction at 80 K at ambient pressure (Finch *et al.*, 1971), and by single-crystal neutron diffraction at 110 K at ambient pressure (Kamb *et al.*, 1971). Early diffraction studies upon ice II within its stability field (*i.e.* under pressure) were carried out using helium as the pressure-transmitting fluid (Arnold *et al.*, 1971). It was immediately recognized that helium must penetrate the ice II structure, since the phase relations (in particular with ice III) did not agree with earlier

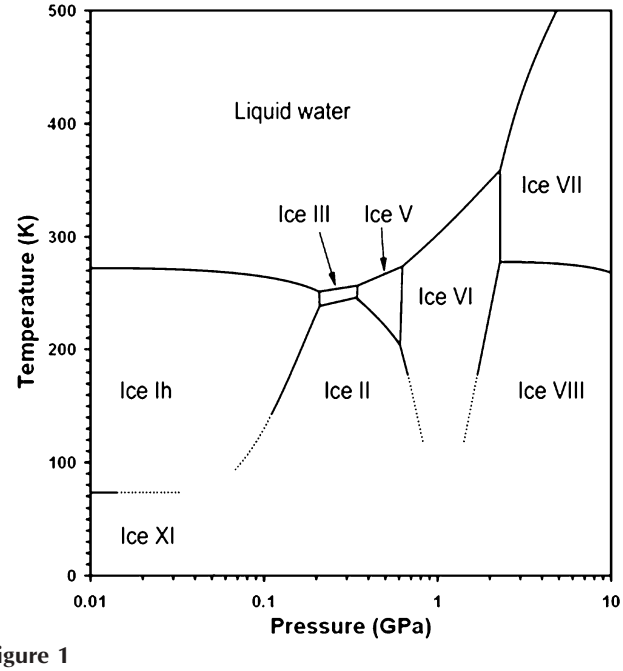

Figure 1
P–T phase diagram of water ice. Observed equilibrium phase boundaries are depicted by solid lines, extrapolated equilibrium boundaries by dashed lines. Note that below ∼100 K, ice II can persist metastably up to ∼5 GPa (Song *et al.*, 2003).

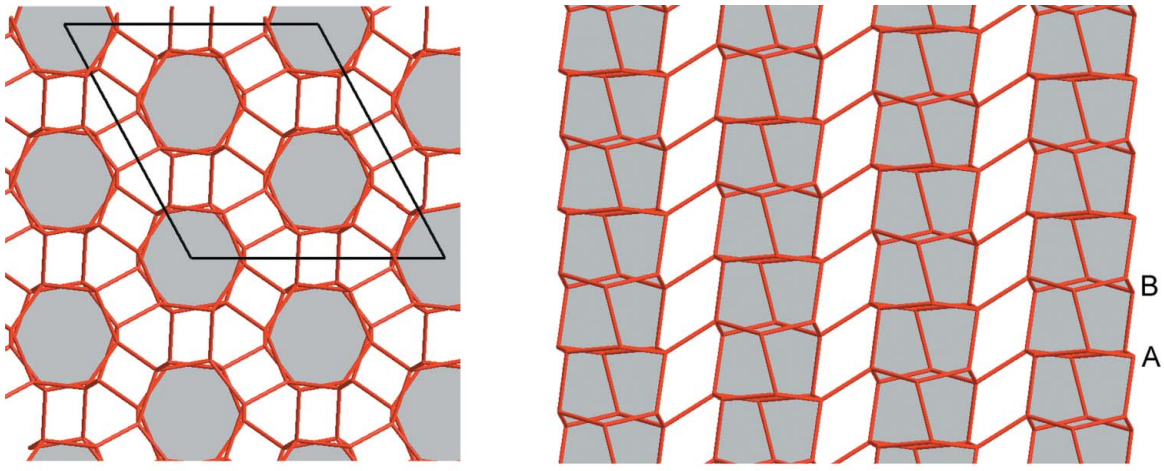

Figure 2
(*a*) A representation of the ice II structure viewed down the *c* axis of the non-primitive hexagonal cell. Observe that the structure consists of a 'sheaf' of hexagonal columns (shaded grey) parallel to the *c* axis. (*b*) A representation of the ice II structure viewed perpendicular to the *c* axis of the non-primitive hexagonal cell, showing the lateral bonding of 6A and 6B rings to join the hexagonal columns (shaded grey) together.

observations. It transpired that helium was forming a 'stuffed ice' helium hydrate which inhibited the formation of ices III and V (Londono *et al.*, 1992, 2002).

Only very recently have diffraction data been collected for 'pure' ice II under pressure, using argon as a pressure-transmitting medium, confirming the ordered structure of the crystal within its stability field above 200 K (Lobban, 1998; Lobban *et al.*, 2002). The crystal structure, shown in Figs. 2(*a*) and 2(*b*), is composed of two varieties of hexagonal rings (hereafter 6A and 6B rings) of hydrogen-bonded water molecules. For the purposes of describing the arrangement of these rings, it is convenient to adopt the non-primitive hexagonal setting of space group $R\bar{3}$: the two types of 6 rings are stacked alternately parallel to the *c* axis, forming six-sided columns, shown in grey. The dangling O–H bonds of the 6A rings extend outwards, although not quite perpendicular to the *c* axis, forming hydrogen bonds from 6A rings in one column to 6B rings in another. The dangling O—H bonds of the 6B rings are directed alternately up and down the *c* axis, although not precisely parallel to it, binding adjacent 6A and 6B rings into columns. This arrangement leads to the 6A rings being relatively flat, and the 6B rings being more corrugated, or puckered. Adjacent rings along the columns are rotated by $\sim 16^\circ$ relative to one another. The structure preserves the open tetrahedral bonding of low-pressure ice I*h*, yet yields a higher density crystal.

The use of argon limits the region of the ice II stability field that one can readily study; the melting point of argon at 0.2 GPa is 128 K, and at 0.5 GPa it is 180 K. Under argon, one can reach limiting low temperatures only by firstly recovering ice II to atmospheric pressure at $\sim$110 K. Our motivation for expanding on the earlier work by carrying out neutron powder diffraction experiments upon ice II was to measure the equation of state, the isothermal bulk modulus and the thermal expansivity. Ice II is likely to be a major rock-forming mineral in the outer Solar System (*e.g.* McKinnon, 1998). Pressure and temperature conditions within a large proportion of the Solar System's icy moons are suitable for the stability of ice II; inside a large icy moon, such as the Jovian satellite Ganymede, ice II may form a layer several hundred kilometres deep. The physical properties of ice II are therefore pertinent to an understanding of the geophysics of icy moons influencing, amongst other things, the convective regimes in their interiors.

Reliable values for the incompressibility do exist, calculated from Brillouin scattering measurements (Gagnon *et al.*, 1990). However, some of the low-temperature compression studies (*e.g.* Bizhigitov, 1987; Sirota & Bizhigitov, 1987, 1988; Sirota & Zhapparov, 1994) did not employ independent phase identification techniques (diffraction or spectroscopy) and so there is an ambiguity as to whether the measurements are of ice II or metastable ice IX. The only diffraction-derived bulk modulus was estimated from two data points (Lobban, 1998; Lobban *et al.*, 2002). The only experimental values for the thermal expansivity are, similarly, estimated from two data points (Lobban, 1998; Lobban *et al.*, 2002). In making accurate determinations of these thermoelastic quantities, we also wished to compare our results with earlier density functional theory calculations of the equation of state (Fortes *et al.*, 2003*a*, 2004; Fortes, 2004), and a point-charge model of the thermal expansion (Báez & Clancy, 1995).

2. Experimental method

Neutron diffraction is probably the best technique for the structural study of hydrogen-bearing crystals, although in practice deuterated analogues must be used to avoid the large incoherent scattering of hydrogen, which contributes to the background of the diffraction pattern (*e.g.* Finney, 1995). Our experiments were carried out at the ISIS facility, a high-flux neutron spallation source located at the Rutherford Appleton Laboratory, Chilton, Oxfordshire, UK, using the High Reso-

lution Powder Diffractometer (HRPD) (Ibberson *et al.*, 1992). Pressure cells composed of either aluminium 7075 alloy or $Ti_{66}Zr_{34}$ null-scattering alloy were used. The aluminium cell has the advantage of shorter data collection times, but the drawback of producing parasitic peaks in the diffraction pattern. Conversely, the TiZr cell requires a longer counting time but contributes no Bragg peaks to the diffraction pattern. Data were collected in the HRPD detector banks at $2\theta \simeq 90^\circ$; collection times adequate for refining the unit-cell volume to better than one part in ten thousand were ∼15 min in the Al cell, and ∼25 min in the TiZr cell.

Liquid D_2O (Aldrich Chemical Co., 99 at.% D) was loaded into the pressure vessel along with a small wad of silica wool to act as a nucleator. The vessel was sealed under ∼50 MPa of argon gas, attached to a cryostat centre stick, and loaded into a vanadium-tailed helium cryostat. The cryostat was mounted in the neutron beamline, and the sample was equilibrated at a temperature of 225 K, which resulted in the formation of polycrystalline ice I*h*. Ice II was then formed by pressurizing the sample, under argon gas, to 0.25–0.27 GPa at 225 K, where the phase transformation takes place in a matter of minutes. Diffraction patterns were collected as a function of pressure within the stability field of ice II at temperatures above the melting line of argon (see below). The sample was then decompressed and recovered to atmospheric pressure at 110 K, after which diffraction patterns were collected in 5 K intervals from 5 to 175 K. Upon warming at ambient pressure, ice II (in common with other quenched high-pressure phases of ice) transforms to the cubic polytype of ice I (ice I*c*, space group $Fd\bar{3}m$; Kuhs *et al.*, 1987); this was observed (in two sample loadings) to occur between 160 and 165 K (see Fig. 3). On one occasion, we warmed ice I*c* to 225 K and compressed it to make a fresh sample of ice II; however, the cubic ice did not transform to ice II until a pressure of 0.35 GPa was applied, and yielded a strongly textured sample.

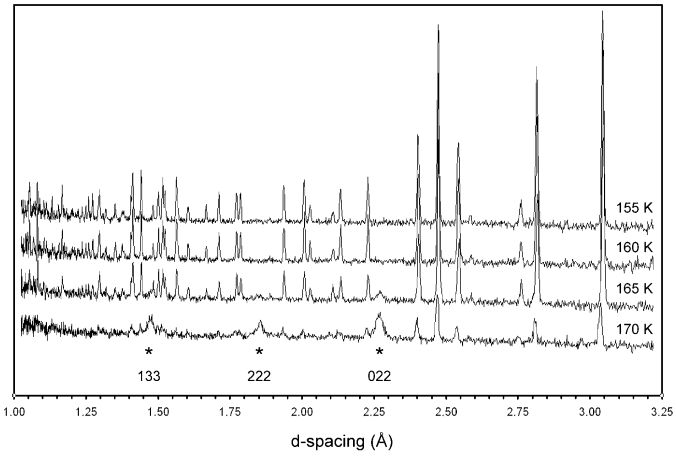

Figure 3
Neutron diffraction patterns collected upon warming ice II through the transition to ice I*c* at 160 K (room pressure). The strongest ice I*c* Bragg peaks are marked with asterisks and their Miller indices. Data were collected in the TiZr pressure cell; each pattern was counted for 25 min in the HRPD 90° banks. No evidence for large-scale amorphization of the sample prior to ice I*c* crystallization was observed.

Table 1
Refined unit-cell dimensions, in the hexagonal setting, for the isothermal compression run described in the text.

Pressure (GPa)	Temperature (K)	*a* (Å)	*c* (Å)	*c*/*a*
0.2502	225	12.9351 (3)	6.2331 (2)	0.4819 (14)
0.2746	225	12.9292 (3)	6.2272 (2)	0.4816 (14)
0.2991	225	12.9230 (3)	6.2222 (2)	0.4815 (14)
0.3251	225	12.9153 (3)	6.2175 (2)	0.4814 (14)
0.3511	225	12.9090 (3)	6.2130 (2)	0.4813 (14)
0.3738	225	12.9034 (3)	6.2083 (2)	0.4811 (14)
0.3991	225	12.8963 (3)	6.2034 (2)	0.4810 (14)
0.4229	225	12.8905 (3)	6.1996 (2)	0.4809 (14)
0.4488	225	12.8842 (3)	6.1951 (2)	0.4808 (14)

In all of the experimental runs, difficulties were encountered with blockages of frozen argon in the pressure capillary running up through the middle of the cryostat centre stick, even when care was taken to warm the capillary. In these instances, we believe that liquid argon, trapped beneath the plug of solid argon, was boiled by the warmth of the sample, generating an overpressure (approximately 0.05 GPa) in the sample space. When this occurred we were unable to determine the pressure acting on the sample and the data had to be discarded. No evidence, in the form of new Bragg peaks, for the formation of argon clathrate was observed during any of the data collection runs; indeed, argon clathrate only formed once during the entire study, at a time when we were endeavouring to melt ice I*h* under ∼50 MPa of Ar gas. Since our runs at high pressure were relatively short, in comparison with the work of Lobban (1998) for example, the lack of clathrate formation is unsurprising.

In three separate loadings (one in the Al cell and two in the TiZr cell), the following usable data sets were collected: in the stability field of ice II we collected data between 0.25 GPa and 0.45 GPa, at 0.025 GPa intervals, along the 225 K isotherm (nine points). At ambient pressure, we collected two sets of data in the Al cell, one from 5 to 80 K (16 points), and the second from 5 to 115 K (23 points). We collected one data set at a pressure of ∼5 kPa in the TiZr cell from 50 to 100 K (11 points), and one nominally at atmospheric pressure from 50 to 160 K (23 points). The unit-cell dimensions were refined using the *CAILS* (*Cell and Intensity Least Squares*) utility in the *Cambridge Crystallographic Software Library* (*CCSL*: Pawley, 1981); the results are tabulated in the hexagonal setting of $R\bar{3}$ in Tables 1 and 2. There were differences in the absolute unit-cell volumes between the four data sets at nominally ambient pressure of about six parts in ten thousand, corresponding to a shift of the sample of ∼0.4 mm; they were therefore normalized such that the unit-cell volumes were identical at 55 K.

3. Results

3.1. Isothermal incompressibility

Diffraction patterns were collected in the TiZr pressure cell at nine pressure points from 0.25 to 0.45 GPa, at 0.025 GPa intervals, along the 225 K isotherm, and refined to yield the unit-cell volume (Fig. 4). These data were fitted with a third-

Table 2
Refined unit-cell dimensions, in the hexagonal setting, for each of the four ambient-pressure warming runs.

The *c*/*a* ratio for all temperatures is 0.483 (1).

Temperature (K)	*a* (Å)	*c* (Å)
Series 1 (Al cell)		
5	12.9035 (3)	6.2338 (2)
10	12.9038 (3)	6.2334 (2)
15	12.9034 (3)	6.2337 (2)
20	12.9036 (3)	6.2338 (2)
25	12.9037 (3)	6.2339 (2)
30	12.9036 (3)	6.2338 (2)
35	12.9041 (3)	6.2340 (2)
40	12.9044 (3)	6.2347 (2)
45	12.9050 (3)	6.2350 (2)
50	12.9054 (3)	6.2357 (2)
55	12.9062 (3)	6.2361 (2)
60	12.9073 (3)	6.2366 (2)
65	12.9087 (3)	6.2373 (2)
70	12.9097 (3)	6.2382 (2)
75	12.9111 (3)	6.2384 (2)
80	12.9124 (3)	6.2396 (2)
Series 2 (Al cell)		
5	12.9039 (3)	6.2340 (2)
10	12.9039 (3)	6.2340 (2)
15	12.9041 (3)	6.2340 (2)
20	12.9040 (3)	6.2340 (2)
25	12.9041 (3)	6.2340 (2)
30	12.9043 (1)	6.2342 (2)
35	12.9046 (3)	6.2343 (2)
40	12.9045 (3)	6.2348 (2)
45	12.9046 (3)	6.2353 (2)
50	12.9051 (3)	6.2356 (2)
55	12.9062 (3)	6.2361 (2)
60	12.9069 (3)	6.2369 (2)
65	12.9083 (3)	6.2376 (2)
70	12.9095 (3)	6.2382 (2)
75	12.9107 (3)	6.2388 (2)
80	12.9123 (3)	6.2395 (2)
85	12.9139 (3)	6.2408 (2)
90	12.9156 (3)	6.2416 (2)
95	12.9174 (3)	6.2425 (2)
100	12.9193 (3)	6.2434 (2)
105	12.9216 (3)	6.2450 (2)
110	12.9236 (3)	6.2460 (2)
115	12.9264 (3)	6.2473 (2)
Series 3 (TiZR cell)		
55	12.9050 (3)	6.2330 (2)
60	12.9060 (3)	6.2335 (2)
65	12.9074 (3)	6.2336 (2)
70	12.9084 (3)	6.2346 (2)
75	12.9096 (3)	6.2352 (2)
80	12.9113 (3)	6.2361 (2)
85	12.9131 (3)	6.2374 (2)
90	12.9148 (3)	6.2377 (2)
95	12.9165 (3)	6.2386 (2)
100	12.9186 (3)	6.2396 (2)
Series 4 (TiZr cell)		
50	12.9050 (3)	6.2315 (2)
55	12.9055 (3)	6.2323 (2)
60	12.9063 (3)	6.2326 (2)
65	12.9073 (3)	6.2331 (2)
70	12.9087 (3)	6.2343 (2)
75	12.9104 (3)	6.2346 (2)
80	12.9117 (3)	6.2358 (2)
85	12.9130 (3)	6.2369 (2)
90	12.9147 (3)	6.2377 (2)
95	12.9164 (3)	6.2390 (2)
100	12.9190 (3)	6.2398 (2)
105	12.9209 (3)	6.2407 (2)
110	12.9226 (3)	6.2420 (2)
115	12.9258 (3)	6.2436 (2)
120	12.9282 (3)	6.2452 (2)
125	12.9308 (3)	6.2465 (2)
130	12.9337 (3)	6.2474 (2)
135	12.9364 (3)	6.2492 (2)
140	12.9398 (3)	6.2508 (2)
145	12.9430 (3)	6.2519 (2)
150	12.9463 (3)	6.2535 (2)
155	12.9500 (3)	6.2552 (2)
160	12.9535 (3)	6.2574 (2)

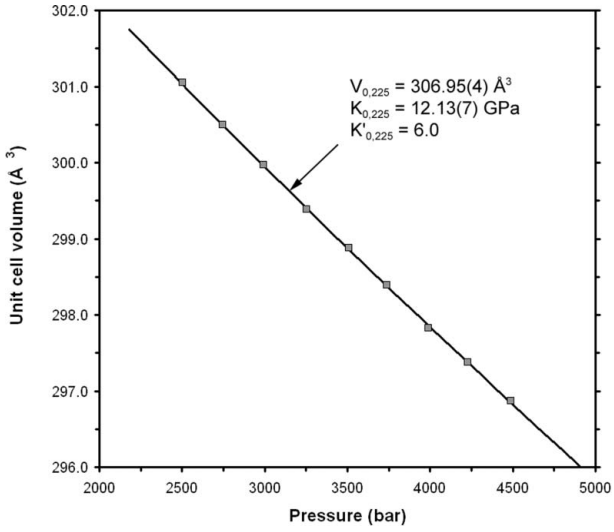

Figure 4
Ice II unit-cell-volume pressure dependence along the 225 K isotherm. The solid line is a third-order Birch–Murnaghan fit to the data (fit parameters are shown). Standard errors on the data points are smaller than the symbols used.

order Birch–Murnaghan equation of state (BMEOS) to yield the following parameters: zero-pressure unit-cell volume, $V_{0,225}$ = 307.36 ± 0.33 Å^3, zero-pressure isothermal bulk modulus, $K_{0,225}$ = 10.9 ± 1.0 GPa, and the first pressure derivative of the bulk modulus, $K'_{0,225}$ = 10 ± 3 (R^2 = 99.987%). Clearly, the narrow pressure range over which the measurements were taken results in poorly constrained values for all three parameters, which are highly correlated. Taking the value $K'_{0,0}$ = 6.0 from *ab initio* calculations (Fortes *et al.*, 2003*a*), yields revised BMEOS3 parameters: $V_{0,225}$ = 306.95 ± 0.04 Å^3 (1299.7 ± 0.2 kg m^{-3}), and $K_{0,225}$ = 12.13 ± 0.07 GPa, with no significant reduction in the quality of the fit; R^2 = 99.983%. [Note that the polynomial function fitted in §3.2 yields an extrapolated value for $V_{0,225}$ of 307.48 ± 0.07 Å^3.]

Previously, Gagnon *et al.* (1990) published a value of 14.39 GPa for the isothermal bulk modulus of H_2O ice II at 0.283 GPa and 237.65 K; Lobban *et al.* (2002) estimated the isothermal bulk modulus of D_2O ice II at 0.35 GPa, 200 K, to be 14.8 ± 0.1 GPa. Our Birch–Murnaghan fit, with $K'_{0,225}$ = 6.0, yields $K_{0.35,225}$ = 14.23 ± 0.07 GPa, which agrees well with the earlier work, and indicates that use of the *ab initio* value for $K'_{0,0}$ is appropriate. The variation of *c*/*a* (Table 1), although within the errors, agrees with the expected degree of isotropy seen in quantum mechanical calculations (Fortes *et al.*, 2003*a*).

The bulk modulus of deuterated ice I*h* at 225 K is 8.9 GPa (Mitzdorf & Helmreich, 1971); ice II is therefore ∼36% stiffer than ice I*h* at the same pressure and temperature. The strength of the intra-ring hydrogen bonds, which according to our *ab initio* calculations (Fortes *et al.*, 2003*a*) resist much of the hydrostatic compression, must therefore more than compensate for weakening of the inter-ring bonds caused by the greater distortion of the O—O—O angles from their ideal tetrahedral value.

3.2. Thermal expansivity

For simple calculations, the unit-cell volumes may be fitted well with a polynomial function (Fig. 5), $V = a_2T^2 + a_1T + a_0$, having coefficients $a_2 = 185.6 \pm 1.1 \times 10^{-6}$, $a_1 = -7.175 \pm 0.176 \times 10^{-3}$, and $a_0 = 299.696 \pm 0.006$ Å^3 ($R^2 = 99.967\%$); the maximum residual between the fit and the data is 0.013%.

Of particular note is the fact that ice II (Fig. 6) does not exhibit the negative thermal expansivity seen in ice I*h* at low temperatures (*e.g.* Röttger *et al.*, 1994), and also that α_V for ice II at 150 K is comparable with that for ice I*h* near 273 K (∼160 $\times 10^{-6}$ K^{-1}); *i.e.* the thermal expansivity of ice II is much larger than that of ice I*h* at a given temperature. Our extrapolated value of α_V at 225 K (at ambient pressure) is 248 $\times 10^{-6}$ K^{-1}, which is comparable with the estimate of Lobban (1998) at 0.4 GPa and 225 K of 261 $\pm$ 2 $\times 10^{-6}$ K^{-1}. The measured thermal expansivity of ice II is also comparable with estimates for other high-density ice polymorphs (Lobban, 1998): ice III ($\alpha_V = 239 \pm 12 \times 10^{-6}$ K^{-1} at 0.25 GPa, 245 K); ice V ($\alpha_V = 240 \pm 5 \times 10^{-6}$ K^{-1} at 0.5 GPa, 245.5 K); and ice XII ($\alpha_V = 270 \pm 5 \times 10^{-6}$ K^{-1} at 0.5 GPa, 257.5 K). Apart from the present study, only ices VII and VIII have had their thermal expansion measured at room pressure (S. Klotz, personal communication), these phases having $\alpha_V \simeq 340 \times 10^{-6}$ K^{-1} at 120 K. It is interesting to observe that there is a continuous increase of α_V with density, reflecting the greater tendency of more compact framework structures to unfold. Both neutron scattering studies (Bennington *et al.*, 1999; Strässle *et al.*, 2004) and computer modelling (Tanaka, 1998; Koyama *et al.*, 2004) show that the negative thermal expansion in ice I*h* is due to low-frequency bond-bending modes with negative Grüneisen parameters; one possible explanation for the lack of negative thermal expansion in ice II is that these modes are significantly weaker in the denser crystal.

The anisotropy of the thermal expansion can be judged by reference to the temperature dependence of the *c*/*a* ratio. The observed change in *c*/*a* as a function of temperature is smaller than 1σ (Table 2) so, as in ice I*h* (see Hobbs, 1974; Röttger *et al.*, 1994), the thermal expansion of ice II is isotropic. This agrees with our *ab initio* calculations (Fortes *et al.*, 2003*a*) where very large compressions (few GPa) produced only very small changes in *c*/*a*.

In order to analyse the thermal expansion data in terms of the fundamental physical properties of ice II, the ambient-pressure data points, after being normalized to yield the same unit-cell volume at 55 K (Fig. 5), were fitted with a second-order approximation to the Grüneisen zero-pressure equation of state (*e.g.* Wallace, 1998), in which the thermal expansion is considered equivalent to elastic strain such that,

$$V(T) = V_{0,0}\left[1 + \frac{E(T)}{Q - bE(T)}\right], \qquad (1)$$

where $V_{0,0}$ is the unit-cell volume at zero pressure and temperature, $b = \frac{1}{2}(K'_{0,0} - 1)$ and $Q = (V_{0,0}K_{0,0}/\gamma)$. $K_{0,0}$ is the zero-pressure and -temperature isothermal bulk modulus, $K'_{0,0}$ is its first derivative with respect to pressure, and γ is a thermal Grüneisen parameter. The internal energy due to lattice

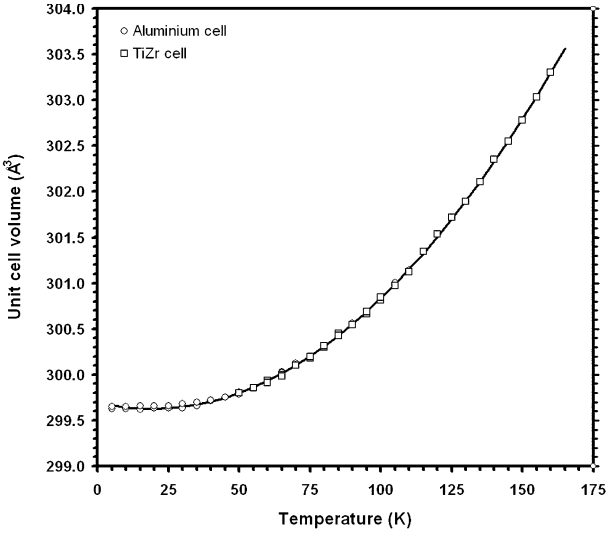

Figure 5
Ice II unit-cell-volume temperature dependence at room pressure. The solid line is a second-order polynomial function fitted to the data (coefficients given in the text).

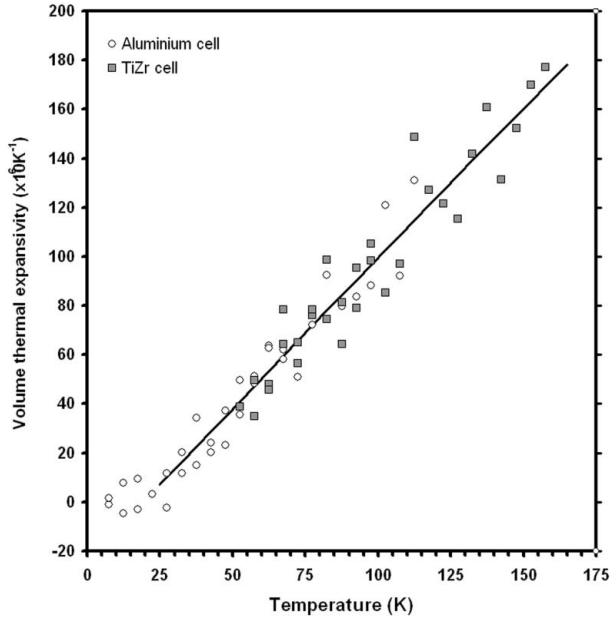

Figure 6
Volume coefficient of thermal expansion, α_V, for metastable ice II at room pressure. Symbols are numerical derivatives of the unit-cell volume data; the solid line is the derivative of the polynomial fit shown in Fig. 4, truncated at 25 K since the fitted second order polynomial does not reproduce the observed asymptotic behaviour.

vibrations, $E(T)$, is determined *via* a Debye model (*e.g.* Ashcroft & Mermin, 1976):

$$E(T) = \frac{9nk_{\rm B}T}{(\theta_{\rm D}/T)^3}\int_0^{\theta_{\rm D}/T}\frac{x^3}{\exp(x)-1}\,{\rm d}x, \qquad (2)$$

where $\theta_{\rm D}$ is the Debye temperature, n is the number of atoms per unit cell, and $k_{\rm B}$ is the Boltzmann constant; the integral term is evaluated numerically. This approach has been previously used with success to model $V(T)$ for 'hard' materials, such as FeSi (Vočadlo *et al.*, 2002) and $KMgF_3$ (Wood *et al.*, 2002). An essentially similar analysis has been proposed as a method for the determination of Debye temperatures by Sayetat *et al.* (1998).

When equation (1) is fitted to our $V(T)$ data the fit is excellent; however, the elastic parameters resulting from the fit are not sensible: $K_{0,0}/\gamma$ = 41.8 GPa and $K'_{0,0}$ = 53.5. As we have found with other hydrogen-bonded crystals, such as $ND_3.2D_2O$ (Fortes *et al.*, 2003*b*) and $MgSO_4.7D_2O$ (report in preparation), the problem lies in the calculation of the internal energy, which is much better represented by two Debye moments with very different characteristic temperatures, $\theta_{\rm D}^{\rm A}$ and $\theta_{\rm D}^{\rm B}$:

$$E(T) = 9nk_{\rm B}\left[X f\left(\frac{\theta_{\rm D}^{\rm A}}{T}\right) + Y f\left(\frac{\theta_{\rm D}^{\rm B}}{T}\right)\right], \qquad (3)$$

where $f(\theta_{\rm D}/T)$ is the Debye function, n is the number of atoms per unit cell, and X and Y are mixing parameters. As no heat capacity measurements for ice II have been published, we tried using the measured heat capacity of ice I*h* (Giauque & Stout, 1936) as a proxy. The parameters resulting from the fitting of equation (3) to the heat capacity data for ice I*h* gave $\theta_{\rm D}^{\rm A}$ = 199 ± 5 K, $\theta_{\rm D}^{\rm B}$ = 1110 ± 6 K, X = 0.211 ± 0.005 and Y = 0.589 ± 0.020. These values are very similar to those of the other hydrogen-bonded crystals we have investigated; the Debye temperatures correspond to vibrational wavenumbers of ∼140 cm^{-1} and 770 cm^{-1} and agree well with the low-frequency edges of the translational and rotational excitations, $\nu_{\rm T}$ and $\nu_{\rm R}$, of the water molecules in ice I*h* (Bertie *et al.*, 1969).

Equation (1) was then refitted to the $V(T)$ data for ice II using the double-Debye model, with $E(T)$ fixed from fitting equation (3) to the ice I*h* heat capacity rather than having $\theta_{\rm D}$ as a free variable. The elastic parameters resulting from this fit are somewhat more sensible: $V_{0,0}$ = 299.592 ± 0.007 Å^3, $K_{0,0}/\gamma$ = 13.74 ± 0.18 GPa, although $K'_{0,0}$ = 57 ± 3. Clearly, the heat capacity of ice I*h* is not a perfect analogue for fitting the internal energy of the ice II crystal, so we decided to reverse the analysis by fixing the elastic properties at sensible values and using the $V(T)$ data to determine the two Debye temperatures; the mixing parameters cannot be independently determined this way. Guided by our *ab initio* calculations (Fortes *et al.*, 2003*a*), we fixed b = 2.5 (*i.e.* $K'_{0,0}$ = 6.0) and Q = 4.0 × 10^{-18} J (*i.e.* $K_{0,0}/\gamma \simeq$ 13.35 GPa), which yielded V_0 = 299.635 ± 0.004 Å^3, $\theta_{\rm D}^{\rm A}$ = 265 ± 19 K, $\theta_{\rm D}^{\rm B}$ = 807 ± 161 K, X = 0.26 ± 0.04, and Y = 0.57 ± 0.12. These Debye temperatures correspond to vibrational wavenumbers of 184 ± 13 cm^{-1} and 561 ± 112 cm^{-1}, respectively, and are not statistically significantly different from the values obtained in fitting to ice I*h*.

4. Discussion and conclusion

At ambient pressure, the experimentally measured unit-cell volume of ice II at 4.2 K is 299.62 Å^3, whereas the value calculated from density functional theory in the athermal limit (Fortes *et al.*, 2003*a*) is 289.43 ± 0.15 Å^3, which differs from the experimental value by −3.4 ± 0.1%. This corresponds to a negative pressure, or dilation, of ∼0.5 GPa, to bring the calculated volume into agreement with the experimental volume. Correcting the bulk modulus calculated from DFT (16.1 ± 0.3 GPa) for this dilation yields a corrected $K_{0,0}$ = 13.0 ± 0.3 GPa, which agrees fairly well with our experimental value.

A point-charge model was used by Báez & Clancy (1995) to calculate the density of ice II from 180–320 K at P = 0. A comparison of their polynomial fit with the present study reveals that their thermal expansivity at 180 K is approximately twice as large as that which we observed experimentally at 160 K. Therefore, work which has used the model of Báez & Clancy (1995) to produce a P–V–T equation of state for ice II (*e.g.* Cruz-León *et al.*, 2002) will be significantly in error.

To summarize, we have measured in detail the isothermal bulk modulus and thermal expansivity of helium-free D_2O ice II for the first time, using high-resolution powder neutron diffraction to confirm the structure and purity of our sample throughout. At 225 K, V_0 = 306.95 ± 0.04 Å^3, K_0 = 12.13 ± 0.07 GPa (assuming K'_0 = 6.0), and $\alpha_{\rm V}$ at P = 0 is predicted, by extrapolation, to be 2.48 × 10^{-4} K^{-1}.

ADF acknowledges a fellowship from the Particle Physics and Astronomy Research Council (PPARC UK), PPA/P/S/2003/00247; MA acknowledges a grant from the Natural Environment Research Council (NERC UK), NER/T/S/2001/00855; LV acknowledges funding by the Royal Society of Great Britain. The authors wish to thank the ISIS Facility for beamtime, and John Dreyer, Andy Church, Chris Goodway and Jon Bones for technical support, as well as two anonymous reviewers for constructive criticism of the manuscript.

References

Arnold, G. P., Wenzel, R. G., Rabindeau, S. W., Nereson, N. G. & Bowman, A. L. (1971). *J. Chem. Phys.* **55**, 589–595.
Ashcroft, N. W. & Mermin, N. D. (1976). *Solid State Physics*. Harcourt Brace College, Orlando, Florida.
Báez, L. A. & Clancy, P. (1995). *J. Chem. Phys.* **103**, 9744–9755.
Bennington, S. M., Li, J. C., Harris, M. J. & Ross, D. K. (1999). *Physica B*, **263**, 396–399.
Bertie, J. E., Calvert, L. D. & Whalley, E. (1963). *J. Chem. Phys.* **38**, 840–846.
Bertie, J. E., Labbé, H. J. & Whalley, E. (1968). *J. Chem. Phys.* **49**, 775–780.
Bertie, J. E., Labbé, H. J. & Whalley, E. (1969). *J. Chem. Phys.* **50**, 4501–4520.
Bertie, J. E. & Whalley, E. (1964). *J. Chem. Phys.* **40**, 1646–1659.

Bizhigitov, T. B. (1987). *Phase Diagram of Ice and Compressibility of its Various Modifications at High Pressure (0–2500 MPa) and Low Temperature (90–300 K)*. PhD Thesis, Moscow.
Bridgman, P. W. (1912). *Proc. Am. Acad. Arts. Sci.* **47**, 441–558.
Bridgman, P. W. (1935). *J. Chem. Phys.* **3**, 597–605.
Bridgman, P. W. (1937). *J. Chem. Phys.* **5**, 964–966.
Cruz-León, G., Rodríguez Romo, S. & Tchijov, V. (2002). *J. Phys. Chem. Solids*, **63**, 843–851.
Finch, E. D., Rabindeau, S. W., Wenzel, R. G. & Nereson, N. G. (1971). *J. Chem. Phys.* **49**, 4361–4365.
Finney, J. L. (1995). *Acta Cryst.* B**51**, 447–467.
Fortes, A. (2004). *Computational and Experimental Studies of Solid in the Ammonia–Water System.* PhD Thesis, University of London.
Fortes, A. D., Wood, I. G., Brodholt, J. P. & Vočadlo, L. (2003*a*). *J. Chem. Phys.* **119**, 4567–4574.
Fortes, A. D., Wood, I. G., Brodholt, J. P., Knight, K. S., Alfredsson, M., McGrady, G. S. & Vočadlo, L. (2003*b*). *J. Chem. Phys.* **119**, 10806–10813.
Fortes, A. D., Wood, I. G., Knight, K. S., Brodholt, J. P., Alfredsson, M. & Vočadlo, L. (2004). *Proc. Lunar Planet. Sci. Conf.* **35**, abstract No. 1252.
Gagnon, R. E., Kiefte, H., Clouter, M. J. & Whalley, E. (1990). *J. Chem. Phys.* **92**, 1909–1914.
Giauque, W. F. & Stout, J. W. (1936). *J. Am. Chem. Soc.* **58**, 1144–1150.
Hobbs, P. V. (1974). *Ice Physics*. Oxford: Clarendon Press.
Ibberson, R. M., David, W. I. F. & Knight, K. S. (1992). *The High Resolution Neutron Powder Diffractometer (HRPD) at ISIS - A User Guide*. Report RAL-92-031, Rutherford Appleton Laboratory, Oxfordshire, UK.
Kamb, W. B. (1964). *Acta Cryst.* **17**, 1437–1449.
Kamb, B. & Datta, S. K. (1960). *Acta Cryst.* **13**, 1029 (abstract 5.63).
Kamb, B., Raymond, C. F., LaPlaca, W. C. & Prakash, A. (1971). *J. Chem. Phys.* **55**, 1934–1945.
Koyama, Y., Tanaka, H., Gao, G. & Zeng, X. C. (2004). *J. Chem. Phys.* **121**, 7926–7931.
Kuhs, W. F., Bliss, D. V. & Finney, J. L. (1987). *J. Phys. C1*, **48**, 631–636.
Lobban, C. (1998). *Neutron Diffraction Studies of Ices.* PhD Thesis, University of London.
Lobban, C., Finney, J. L. & Kuhs, W. F. (2002). *J. Chem. Phys.* **117**, 3928–3934.
Londono, J. D., Finney, J. L. & Kuhs, W. F. (1992). *J. Chem. Phys.* **97**, 547–552.
McFarlan, R. L. (1936*a*). *J. Chem. Phys.* **4**, 60–64.
McFarlan, R. L. (1936*b*) *Rev. Sci. Instrum.* **7**, 82–85.
McKinnon, W. (1998) *Geodynamics of Icy Satellites.* In *Solar System Ices*, edited by B. Schmitt, C. de Bergh & M. Festou. Dordrecht: Kluwer Academic Publishers.
Mitzdorf, U. & Helmreich, D. (1971). *J. Acoust. Soc. Am.* **49**, 723–728.
Pawley, G. S. (1981). *J. Appl. Cryst.* **14**, 357–361.
Röttger, K., Endriss, A., Ihringer, J., Doyle, S. & Kuhs, W. F. (1994). *Acta Cryst.* B**50**, 644–648.
Sayetat, F., Fertey, P. & Kessler, M. (1998). *J. Appl. Cryst.* **31**, 121–127.
Sirota, N. N. & Bizhigitov. T. B. (1987). *Dokl. Akad. Nauk SSSR*, **297**, 1112–1116.
Sirota, N. N. & Bizhigitov. T. B. (1988). *Cryst. Res. Technol.* **23**, 595–603.
Sirota, N. N. & Zhapparov, K. T. (1994). *Dokl. Akad. Nauk SSSR*, **334**, 577–580.
Song, M., Yamawaki, H., Fujihisa, H., Sakashita, M. & Aoki, K. (2003). *Phys. Rev. B*, **68**, 024108.
Strässle, Th., Saitta, A. M., Klotz, S. & Braden, M. (2004). *Phys. Rev. Lett.* **93**, 225901.
Tammann, G. (1900). *Ann. Phys. (IV)*, **2**, 1–31.
Tanaka, H. (1998). *J. Chem. Phys.* **108**, 4887–4893.
Vočadlo, L., Knight, K. S., Price, G. D. & Wood, I. G. (2002). *Phys. Chem. Min.* **29**, 132–139.
Wallace, D. C. (1998). *Thermodynamics of Crystals*. New York: Dover.
Whalley, E. & Davidson, D. W. (1965). *J. Chem. Phys.* **43**, 2148–2149.
Wilson, G. J., Chan, R. K., Davidson, D. W. & Whalley, E. (1965). *J. Chem. Phys.* **43**, 2384–2391.
Wood, I. G., Knight, K. S., Price, G. D. & Stuart, J. A. (2002). *J. Appl. Cryst.* **35**, 291–295.